Optical Spectra of Cu, Ag, and Au Monomers and Dimers at Regular Sites and Oxygen Vacancies of the MgO(001) Surface. A Systematic Time-Dependent Density Functional Study Using Embedded Cluster Models†

Sergey I. Bosko, Lyudmila V. Moskaleva,* Alexei V. Matveev, and Notker Rösch*

Department Chemie, Technische Universität München, 85747 Garching, Germany

Received: January 14, 2007; In Final Form: March 18, 2007

Polarization-resolved optical spectra of coinage metal monomers and dimers M_n (M = Cu, Ag, Au; $n = 1$, 2) at ideal O^{2-} sites of MgO(001) as well as at oxygen vacancies, F_s and F_s^+, of that surface were established using a computational approach based on linear response time-dependent density functional theory. Calculations were performed for structures determined by applying a generalized-gradient density functional method to cluster models embedded in an elastic polarizable environment. This embedding scheme provides an accurate description of substrate relaxation and long-range electrostatic interaction. We compared the optical properties of adsorbed atoms and dimers with those of the corresponding gas-phase species and we systematically analyzed trends among congeners.

1. Introduction

Unique optical, thermodynamic, electronic, and spectral properties of metal nanoparticles have made them useful in different applications, such as optical and electronic devices, optical data storage, biosensors, magnetism, catalysis.[1−4]

In this context, metal nanoclusters supported on oxide surfaces and thin films as well as on inner surfaces of zeolite frameworks attract growing interest,[5,6] as there is an obvious advantage of incorporating very small amounts of clusters with special chemical and physical functions into conventional materials, which in addition provide structural support for the clusters. However, the support itself may affect electronic structure and chemical properties of supported species.[5,7] In particular, surface defects have been shown to influence in a direct and characteristic fashion the properties of adsorbed species due to typically stronger interaction with these sites than with more chemically inert regular positions.[5,7] Cluster-support interaction is thus a crucial issue when rationalizing observations on such systems and using this knowledge in the design of new materials with predefined properties.

Although chemical and catalytic properties of supported metal nanoparticles comprise an area of intensive and fruitful research,[5,6,8] experimental or theoretical studies on magnetic[9] and optical properties[10−14] of deposited nanoparticles are far less numerous. However, this situation is changing fast due to the growing recognition of the potential for using the practically attractive optical properties of metal nanoclusters (in particular Au, Ag, and nanoalloys thereof) in the design of materials with desired optical response for applications like tagging and anticounterfeiting (or "labeling") technology, plasmonics,[15] optical communications, and optical information processing.[16]

In addition to practical applications just mentioned, optical transitions of clusters provide characteristic signatures that can be exploited in experimental characterization techniques. Optical spectroscopy has long been used to study metal clusters in the gas phase.[2,17] However, studies on supported clusters require the development of new characterization tools to complement those of traditional surface science, such as UPS-XPS or EELS, for which major challenges arise due to the low concentrations of adsorbed species (at the border of detection limit) and the dominant background signal of the support material. Only recently was the very sensitive cavity ringdown spectroscopy (CRDS) applied to surface systems, and it seems to emerge as a method of choice for overcoming these problems.[13,14]

Theoretical investigations of absorption spectra of supported metals represent a complex task, which can be performed with sufficient accuracy with the help of the linear response time-dependent density functional (TDDFT) method.[18] The potential of this theoretical approach for surface systems has not yet been fully exploited; among the few published works we mention very recent contributions devoted to Cu or Au atoms and small aggregates on MgO[11,12] and atomic and dimer Au species on amorphous SiO_2.[13,14]

Recently, our group carried out a series of systematic adsorption studies[19−23] on coinage metal atoms and small aggregates, M_n (M = Cu, Ag, Au, $n = 1-4$), deposited at regular O^{2-} and oxygen vacancy sites F_s or F_s^+ of MgO(001). In continuation of these studies, we present here a systematic evaluation and discussion of the optical absorption spectra of supported coinage metal atoms and dimers, where we explored three key parameters: elemental composition, particle size, and interaction with the support on regular as well as defect sites. In the size range where metal particles consist of only a few atoms, the optical properties of free and supported clusters are directly linked to their intrinsic electronic and geometric properties. We will show that for such small supported species, interaction with a defect can significantly affect their electronic energy levels and optical signatures.

2. Computational Methods and Models

The properties of atoms M_1 (M = Cu, Au, Ag) and dimers M_2 adsorbed at O^{2-} sites of the regular MgO(001) surface as well as at F_s and F_s^+ oxygen vacancies of that surface were theoretically studied in the framework of density functional

† Part of the special issue "M. C. Lin Festschrift".

* Corresponding authors. E-mail: N.R., roesch@ch.tum.de; L.V.M., moskaleva@ch.tum.de.

10.1021/jp070303g CCC: $37.00
Published on Web 05/04/2007

theory with the help of the parallel computer code ParaGauss.[24,25] All-electron calculations were carried out with the linear combination of Gaussian-type orbitals fitting-functions density functional (LCGTO-FF-DF) method.[26] We used a generalized gradient approximation (GGA) of the exchange-correlation (xc) potential suggested by Becke and Perdew (BP86).[27] Local density approximations (LDA) and GGA of the xc potential are known to yield rather similar results in TDDFT calculations of excitation energies.[18]

The calculations were performed at the nonrelativistic level for Cu and with the scalar relativistic variant of the Douglas−Kroll−Hess approach to the Dirac−Kohn−Sham problem for Ag and Au.[28] Thus, the current study does not account for spin−orbit (SO) interaction. Optical properties of free and adsorbed atoms and dimers were computed using a linear response formalism based on the time-dependent density functional theory (TDDFT) as implemented in the program ParaGauss.[24,29] That module was recently extended[30] for application to spin-polarized systems and full use of spatial symmetry.[31] For numerical stability, the resolution of the identity in the coupled Kohn−Sham equations[29] was applied only to the Coulomb part of the response kernel and the xc contribution to the response kernel was treated by an accurate numerical integration.[30]

The Gaussian-type orbital basis sets of Cu, Ag,[32a] and Au,[32b] used in the structure optimization,[19−21] had to be augmented by diffuse functions for an accurate evaluation of absorption properties by the linear response TDDFT method. The orbital basis set of Cu was augmented by one s exponent (0.012237 au), two p exponents (0.046199, 0.021537 au), and one d exponent (0.042600 au). The orbital basis set of Ag was augmented by two s exponents (0.041877, 0.014877 au), and two p exponents (0.032648, 0.012615 au). Similarly, the orbital basis set for Au atom was augmented by one s exponent (0.004545 au) and three p exponents (0.008695, 0.003780, 0.001644 au). Thus, in the TDDFT calculations, the orbital basis sets of the coinage metal atoms were Cu(16s13p7d → 7s5p4d), Ag(19s15p9d → 8s6p5d), and Au(22s20p11d7f → 9s7p6d4f). For the support, we used the same orbital basis set, Mg-(15s10p1d → 6s5p1d) and O(13s8p1d→6s5p1d),[26] as in earlier studies.[19−23] The generalized atomic contractions were obtained from BP86 calculations on atoms. For additional flexibility of the wave functions in the cavity of the surface defects, F_s or F_s^+ centers were represented by a "ghost" basis set of oxygen.[21]

The auxiliary basis set used in the LCGTO-FF-DF method to represent the electron charge density and for treating the Hartree part of the electron−electron interactions was constructed in a standard fashion.[26] The s and p exponents of the orbital basis sets were doubled for s- and r^2-type functions of the auxiliary basis set. In addition, five "polarization" exponents of p- and d-type were added on each atom, constructed as geometric series with a factor 2.5. The exponents of the p set started at 0.1 au for Mg and O, 0.133442 au for Cu, and 0.103053 au for Ag as well as Au; the corresponding d-type series started in each case at twice these values. The resulting auxiliary basis sets were Cu(16s,13r^2,5p,5d), Ag(19s,15r^2,5p,-5d), Au(22s,20r^2,5p,5d), Mg(13s,4r^2,5p,5d), O(13s,4r^2,5p,5d).[19−23] The influence of additional auxiliary functions on the excitation spectra under scrutiny, in particular of diffuse p- and d- or higher angular momenta f- and g-functions, proved to be rather minor. A study of metal atoms and dimers in the gas phase and on selected support sites demonstrated that the use of saturated auxiliary basis sets (at least 13 exponents each of p-, d- and f-type) resulted in differences of 0.01−0.06 eV for excitation energies and 0.005−0.010 for oscillator strengths.

The spatial grids for numerical integration of xc contributions in SCF and response calculations were set up as a superposition of radial and angular grids.[33] The radial grids comprised 102 shells for Cu, 119 shells for Ag, and 102 shells for Au, 67 shells for Mg, and 29 shells for O anion. In each shell a Lebedev angular grid accurate up to angular momentum $L = 23$ for the coinage metal atoms, and $L = 17$ for the substrate atoms was used.[34]

Cluster models of the MgO substrate, described quantum mechanically (QM), were embedded in an elastic polarizable environment (EPE), represented by a force field.[35] The EPE approach to cluster model embedding affords an accurate description of the relaxation of the support also for a charged defect, F_s^+. We employed the QM cluster $Mg_9O_9(Mg^{PP})_{16}$ to model adsorption of atoms at O^{2-} sites of the regular MgO-(001) surface and the QM cluster $Mg_9O_8(Mg^{PP})_{16}$ for atomic adsorption at neutral, F_s, and charged, F_s^+, oxygen vacancies.[19,20] Here, Mg^{PP} designates pseudopotential centers Mg^{2+} without electrons.[35] For dimers, we used slightly different cluster models, $Mg_{10}O_{10}(Mg^{PP})_{12}$ and $Mg_9O_8(Mg^{PP})_{12}$, respectively.[21] In all cases studied, the coinage metal atom or dimer adsorbed directly above an O atom or a corresponding oxygen vacancy. The optimized geometries were taken as determined in previous studies.[19−21] All cluster models with adsorbed atoms were calculated in C_{4v} symmetry, and cluster models for adsorbed dimers were calculated in C_s symmetry.

In the molecular orbital (MO) analysis given below, we will use a simplified terminology where we refer to a MO according to its leading (zero-order) character. In important cases, we will explicitly comment on admixtures of other orbitals. Also, we will assign electronic transitions by their dominant contribution; of course, TDDFT calculations commonly yield many, often notably smaller contributions from other symmetry-allowed combinations of states.

Calculated polarization-resolved optical spectra will be presented with a Gaussian broadening ($\sigma = 0.05$ eV equivalent to a full width of 0.12 eV at half-height) applied to individual transitions weighted by the corresponding calculated oscillator strengths.

3. Results and Discussion

3.1. Optical Transitions of M_1 Adsorbed at Regular and Defect Sites of MgO(001). *Atoms in the Gas Phase and at Regular O^{2-} Sites.* Our own studies[19−21,36] and those by others[11,37] have unambiguously shown that metals preferentially adsorb on top of a surface oxygen anion. The nature of interaction with the regular surface sites is mainly polarization and electrostatic attraction, counteracted by Pauli repulsion; therefore, adsorption energies are moderate, 93, 46, and 96 kJ mol^{-1}, for Cu, Ag, and Au, respectively.[19,20] Distances to the oxygen center forming the adsorption site are 2.11, 2.29, and 2.30 Å, for Cu, Ag, and Au, respectively. Two TDDFT studies recently addressed optical properties of Cu[11] and Au[12] atoms and larger aggregates supported at regular O^{2-} and F_s sites of MgO(001) terraces. However, neither a theoretical nor an experimental work to date compared systematically the optical spectra of the coinage metals adsorbed at MgO. The current work attempts such a systematic evaluation. We also wanted to compare with the results of earlier TDDFT studies for Cu and Au,[11,12] where different types of pseudopotential approaches were used in contrast to the present all-electron method; in ref 12, a plane-wave based technology[38] was employed as opposed to the present approach which relies on localized MO basis sets.

TABLE 1: Vertical Transition Energies (eV) and Oscillator Strengths (in Square Brackets) for Coinage Metal Atoms in the Gas Phase (gp) and Supported at O^{2-} Sites of MgO(001)[a]

		$(n-1)$d → ns		ns → np		ns → $(n+1)$s	
		calc	exp[b]	calc	exp[b]	calc	exp[b]
Cu	gp	1.10 (H_g) [0.000]	1.49	4.12 (T_{1u}) [0.154]	3.81	5.18 (A_g) [0.000]	5.35
	O^{2-} site	2.13 (E) [0.001]		2.45 (E) [0.072]		3.41 (A_1) [0.076]	
		2.20 (A_1) [0.000]		2.86 (A_1) [0.004]			
		2.36 (B_2) [0.000]					
		2.39 (B_1) [0.000]					
Ag	gp	3.27 (H_g) [0.000]	3.97	4.07 (T_{1u}) [0.234]	3.74	5.14 (A_g) [0.000]	5.28
	O^{2-} site	2.66−5.44 [0.053][c]		2.62 (E) [0.110]		3.54 (A_1) [0.053]	
				3.22 (A_1) [0.133]			
Au	gp	1.36 (H_g) [0.000]	1.74	5.23 (T_{1u}) [0.129]	4.95	6.16 (A_g) [0.000]	6.76
	O^{2-} site	2.14−5.15 [0.012][c]		3.33 (E) [0.041]		4.20 (A_1) [0.046]	
				3.87 (A_1) [0.038]		4.26 (A_1) [0.049]	
						4.28 (A_1) [0.042]	

[a] Atoms in the gas phase were calculated in I_h symmetry, adsorbed atoms in C_{4v} symmetry. The irreducible representations given in parentheses characterize the transition dipole moment. [b] Reference 39. Experimental values for d → s and s → p transitions are averaged over the fine structure. For transitions between degenerate states, oscillator strengths per partner are given. [c] Maximum value.

To understand the nature and trends in optical transitions of adsorbed coinage metal atoms, it is informative first to look at the excitation spectra of the corresponding free species. All three congeners, Cu, Ag, and Au, feature the same electronic ground state ^{2}S and electronic configuration of the valence shell, $(n-1)d^{10}ns^1$ (with $n = 4, 5, 6$, respectively). The low-lying excited states include ^{2}D, ^{2}P, and $(n+1)$s ^{2}S obtained by promoting a single electron: $(n-1)$d → ns, ns → np, and ns → $(n+1)$s, respectively (Table 1);[39] of these excitations, only ns → np transitions are symmetry allowed in optical spectra. Promoting one d electron into the valence p shell results in dipole forbidden high-spin states ^{4}P, ^{4}F, and ^{4}D, which for Cu and Au, extend in part below the $(n+1)$s ^{2}S level. The 5d → 6p excitations of Au are strongly affected by spin−orbit interaction; for instance, the three components of ^{4}P, with a weighted average of 5.66 eV, are separated by 1.4 eV due to spin−orbit interaction.[39] Table 1 compares calculated excitation energies for free atoms with experimental data obtained by averaging term energies over the spin−orbit structure and also with the excitation energies for supported atoms to be discussed below. The $(n-1)$d → np group of transitions is not included because for atoms supported at O^{2-} sites of MgO this series lies above the presently considered energy range up to 4.5 eV.

That energy range is already at the border of the theoretical band gap of MgO(001), 4.6 eV, as determined with the presently used GGA method, whereas the experimental gap is much larger, 7.8 eV.[40] Common local density functional and GGA methods are known to underestimate the band gap of wide-gap insulators.[41] Unfortunately, this causes some artifacts (and we will touch on that again in the further discussion), e.g., unrealistic mixing of unoccupied levels of the metal with the conduction band of the support. Hence, only the lowest transitions can be reliably and unambiguously described with the methodology used here. Our GGA estimate for the band gap of the support is close to the value, 4 eV, previously estimated with a cluster approach at the LDA level.[12] Therefore, it would not be appropriate if we tried to match blindly current TDDFT results to experimental data. Instead of expecting quantitative accuracy, we regard the current computational method as a semiquantitative tool, which affords a coherent systematic comparison and information about the MOs involved in the various transitions. In this way, it may become useful for interpreting experimental results. Also, the method provides valuable means for assessing trends; e.g., it allows us to compare systematically the three coinage metals and to explore the extent to which the cluster geometry as well as the nature of the adsorption site affects general aspects of spectral features.

As seen from Table 1, for free atoms the current TDDFT approach reproduces experimental trends very well: the order and the relative energies of the transitions are adequately predicted. The maximum error in the theoretical transition energies, ∼25%, is obtained for the 3d → 4s transition of Cu, but the average deviation from experiment, 12%, is quite a bit smaller. We note a significantly larger separation of 4d and 5s levels in the Ag atom, ∼4 eV, compared to the corresponding valence levels in Cu and Au, 1.5 and 1.7 eV, respectively. The similarity between Cu and Au comes as the consequence of a relativistic stabilization of the 6s and simultaneous destabilization of the 5d levels of Au.[42] The same trend also occurs for bulk metals, where the 4d levels of bulk Ag were found to lie ∼2 eV lower than the 3d levels of bulk Cu;[43] the 5d levels of bulk Au lie ∼1 eV below the 3d levels of bulk Cu.[44]

As a result of the interaction with the O^{2-} anions of the MgO surface, the ns level of the coinage metal atom M shifts to higher energies; this effect is a manifestation of the so-called Pauli repulsion between the filled shells. Consequently, ns → np and ns → $(n+1)$s transition energies are reduced by 1.5−2 eV (Table 1). In addition, the M np levels split into p_z and $p_{x,y}$ components; the former level also shifts to a somewhat higher energy due to electrostatic destabilization by a negatively charged oxygen center.

Figure 1 shows the calculated polarization-resolved absorption spectra for Cu, Ag, and Au monomers adsorbed on top of an O center of the ideal MgO(001) surface. The three main spectral features, labeled by I, II, and III, are the same for all three metals M and have mainly intra-atomic character, ns → $np_{x,y}$, ns → np_z, and ns → $(n+1)$s, respectively. However, the unoccupied np and $(n+1)$s levels of the coinage metal M lie rather close to the upper end of the MgO band gap and mix considerably with unoccupied states of the support. For instance, the $4p_z$ level of Cu delocalizes particularly strongly via mixing with several unoccupied states. Consequently, it contributes to several transitions, of which the lowest most intensive ones are marked as II and III. The M np_z level also mixes strongly with higher lying states of M s character. Yet for simplicity, in Table 1, transitions II and III are formally assigned as ns → np_z or ns → $(n+1)$s according to our convention (see section 2). In contrast, the ns → $np_{x,y}$ transitions are quite unambiguously identified, as can be seen from polarization-resolved spectra (Figure 1).

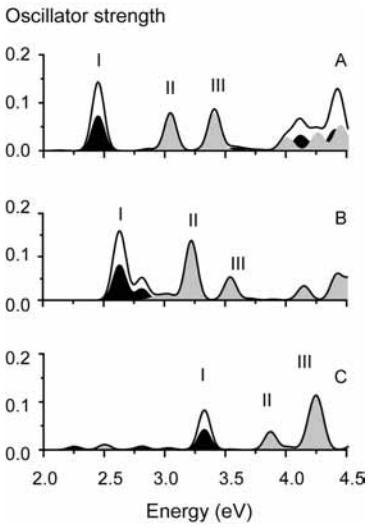

Figure 1. Absorption spectra of coinage metal atoms Cu (A), Ag (B), and Au (C) adsorbed at an O^{2-} site of a defect-free MgO(001) surface. Spectra are weighted by calculated oscillator strengths and broadened by a Gaussian with $\sigma = 0.05$ eV. Polarization-resolved spectra are indicated by shading: gray, *z*-polarized transitions; black, one of two equal polarization components of *xy*-polarized transitions. See the text for a discussion of the major peaks marked with I, II, and III.

These transitions are of E symmetry within the C_{4v} point group and thus are "visible" in *x* or *y* polarized light.

The d → s transitions, which were symmetry forbidden for atoms, now appear with low intensity due to mixing with the states of the support, e.g., a feature at ∼2.8 eV for Ag (Figure 1B) and at ∼2.5 eV for Au (Figure 1C). The mixing of the metal d states with the top of the O 2p valence band is especially pronounced for silver. This is also consistent with our observations for the free Ag atom and the bulk metal (see above), where we noted lower lying 4d levels of Ag compared to the corresponding $(n-1)$d levels of Cu and Au. Figure 2A displays the calculated density of states (DOS) of Ag adsorbed at an O^{2-} site of a defect-free MgO(001) surface, represented by a $Mg_9O_9(Mg^{PP})_{16}$ embedded cluster model; the contributions to the total DOS from d, s, and p states of the Ag atom are explicitly given. The other two coinage metals show qualitatively similar patterns. The singly occupied *n*s orbital of each of the three adsorbed monomers lies well inside the band gap of MgO, whereas the $(n-1)$d and *n*p levels appear at the lower and upper ends of the band gap, respectively. The 6s orbital of an adsorbed Au atom is shifted by ∼1 eV to lower energies compared to Ag and Cu. Hence, the three major signals of Figure 1 (all originating from the *n*s level of M) are shifted to higher energies for Au_1/MgO (panel C). The unlabeled features to the far right of panels A and B can be roughly assigned to transitions of type *n*s → $(n+1)$p and $(n-1)$d → *n*p. However, these high-lying transitions can no longer be unambiguously described in terms of excitations within a metal atom as the corresponding final states involve notable admixtures of the support which likely have to be considered as artifacts of the presently used xc approximation.

Some of the present findings can be compared to the results of other recent TDDFT studies.[11,12] In the previous study on Cu_1/MgO, only the 3d → 4s and one of the 4s → 4p transition energies are given.[11] That prediction at the B3LYP level is very close to our result: 2.29−2.57 eV vs 2.13−2.39 eV of this work for the 3d → 4s transitions and 2.63 eV vs 2.45 eV of this work for the lowest 4s → 4p transition (we assigned this transition to 4s → $4p_{x,y}$). An optical spectrum of Au_1/MgO was recently

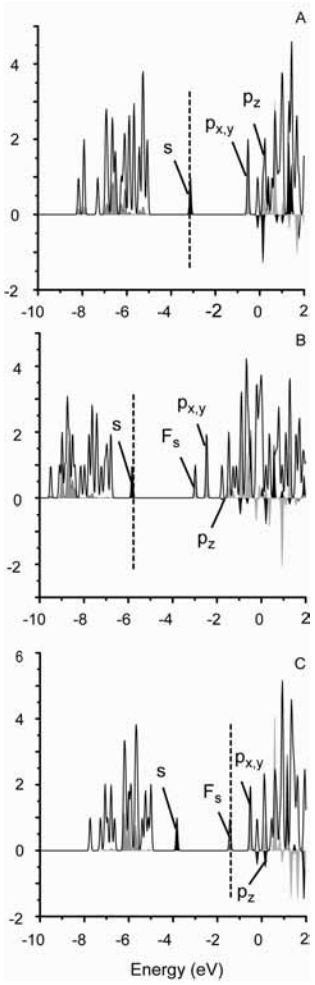

Figure 2. Density of states for Ag_1 adsorbed at various sites of MgO-(001): (A) regular O^{2-} site; (B) F_s^+ site; (C) F_s site. A Gaussian broadening with $\sigma = 0.05$ eV was applied. Contributions from Ag s, p, and d orbitals are given by black, light gray, and dark gray shading, respectively. The position of the highest occupied Kohn−Sham level is marked by a vertical dashed line.

reported from a TDLDA calculation;[12] there, the first two strong transitions were also assigned to 6s → 6p excitations, split into $p_{x,y}$ and p_z components. Given the rather different computational methodologies, the TDLDA excitation energies at 3.38 and 3.61 eV agree very well with the present results, 3.33 and 3.87 eV.

Atoms at F_s^+ Vacancy Sites. "Color centers" F_s^+ or F_s are point defects on a surface that correspond to oxygen vacancies with one or two free electrons, respectively, trapped in a cavity previously occupied by a missing O atom. The bonding of M_1 to an F_s^+ center[45] can be envisioned as interaction of the singly occupied vacancy level and the *n*s and *n*p_z orbitals of M, particularly strongly with *n*p_z; as schematically illustrated in Figure 3, this is a typical example of a three-orbital interaction.[46] The *n*s orbital of M shifts down, whereas the F_s and *n*p_z levels shift up. Note the nonbonding character of the intermediate level, which we refer to as F_s (level); actually, it carries a strong M p_z contribution. The orbital labeled p_z has a contribution of the original F_s cavity level. Therefore, our notations reflect the nature of these MOs only approximately. As a result of such interaction, the *n*s orbital of an adsorbed metal atom becomes doubly occupied and the F_s cavity level is formally empty if adsorption occurs at a charged defect, F_s^+. Favorable bonding of M_1 at an F_s^+ center is manifested by metal adsorption energies that are 2−5 times larger than the binding energies at regular O^{2-} sites of MgO(001).[19,20] Compared with binding energies

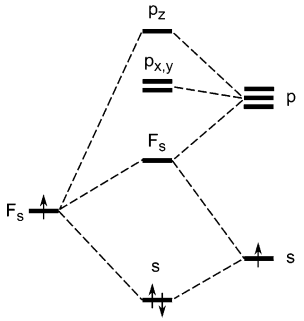

Figure 3. Schematic orbital energy diagram illustrating the interaction of a metal M_1 with an F_s^+ site at the MgO(001) surface.

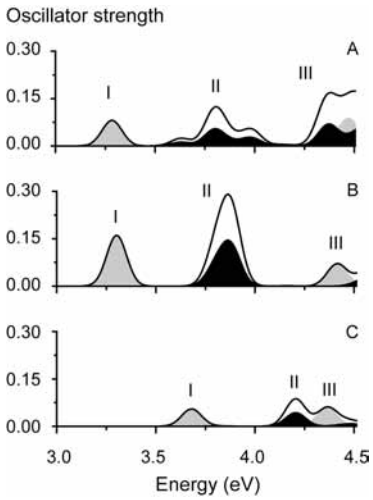

Figure 4. Absorption spectra of coinage metal atoms Cu (A), Ag (B), and Au (C) adsorbed at an F_s^+ site of the MgO(001) surface. Polarization-resolved spectra are indicated by shading; layout is as in Figure 1. See the text for a discussion of the major peaks marked with I, II, and III.

of 242 and 229 kJ mol^{-1} for Cu and Ag, respectively, the Au monomer features the strongest interaction, 358 kJ mol^{-1}, which correlates with the fact that the Au 6s orbital is ~1 eV lower in energy than Cu 4s or Ag 5s in either free atoms or atoms adsorbed on regular O^{2-} sites of MgO(001), as shown by our calculations. Consequently, the stabilization due to electron transfer from the vacancy site is stronger for Au.

As seen from Figure 2B, the ordering of frontier orbitals slightly changes upon going from M_1/O^{2-} to M_1/F_s^+. The *n*s → *n*p separation grows somewhat larger, but the F_s orbital, with a notable M *n*p_z contribution, appears below the M *n*$p_{x,y}$ levels. Thus, at variance with the optical spectra of M_1 adsorbed at O^{2-} sites, the *n*s → F_s(*n*p_z) transition (I in Figure 4) occurs at lower energies than the *n*s → *n*$p_{x,y}$ transition (II in Figure 4). The next group of transitions, III, can be classified as predominantly (n − 1)d → *n*$p_{x,y}$. Recall that our model neglects spin−orbit interaction, which should shift the initial state to somewhat higher energies. Less intensive (n − 1)d → *n*p_z transitions have lower energy and overlap with *n*s → *n*$p_{x,y}$ bands. For Au_1 on F_s^+, the energy separation of excitations with initial states of 5d and 6s character is really small (below 1 eV); thus, one observes in Figure 4 that bands II and III, quite well separated for Cu and Ag, almost overlap for Au. Transitions of type *n*s → *n*p_z(F_s) and *n*s → (n + 1)s lie higher than 5 eV and are not discussed here.

The difference to optical spectra of M_1 adsorbed at O^{2-} sites is quite pronounced. The first strong transitions in the case of M_1/F_s^+ appear at higher energies than in the case of M_1/O^{2-}. Furthermore, a fundamental difference in the spectral pattern is most easily recognized if one compares polarization-resolved contributions to the spectra (Figures 1, 4).

Atoms at F_s Vacancy Sites. The interaction of a neutral vacancy site with an adsorbed coinage metal atom follows the same scheme as described above for the case of F_s^+ (see Figure 3) with the essential difference that the vacancy contributes an additional electron. Therefore, the HOMO of the ground state is the singly occupied F_s(*n*p_z) level.

Accordingly, the lowest transitions originate from the F_s level (Table 2). Spectral features for Cu, Ag, and Au in the low-energy region are quite similar (Figure 5). The low-intensity peak I corresponds to F_s → *n*$p_{x,y}$ transitions, whereas peak II is assigned to a transition from F_s to a level exhibiting mainly MgO character. This probably is an artifact of the model as in reality the bottom of the MgO conduction band should lie much higher than predicted by our GGA-based TDDFT approach. The most intensive band III is a transition from F_s to *n*p_z, followed by F_s → (n + 1)$p_{x,y}$ (IV) and higher lying transitions involving higher order p and s levels of M, which contain a sizable contribution from unoccupied levels of MgO. Thus, beyond that point application of our GGA-based TDDFT method is not very meaningful. Overall, a notable difference to optical spectra of coinage metal atoms adsorbed at regular O^{2-} sites and F_s^+ sites is that intense peaks appear in our model at much lower energies, at 1.5 eV or below. Polarization-resolved spectra below 2.5 eV are dominated by transitions polarized in the *z*-direction, i.e., perpendicular to the surface plane.

3.2. Optical Transitions of Coinage Metal Dimers Adsorbed at Regular and Defect Sites of MgO(001). *Dimers in the Gas Phase and at Regular O^{2-} Sites.* The dimers Cu_2, Ag_2, and Au_2 in the gas phase are characterized by a singlet ground state, $^1\Sigma_g^+$.[47] The order of the valence orbitals as obtained at our BP86 level is similar for Cu_2 and Au_2 and involves an antibonding combination of d orbitals, dσ_u* orbital, as the HOMO (Figure 6), and the antibonding combination, sσ_u*, as the LUMO. This is different from the MO ordering rendered by HF-based methods[48,49] and the hybrid B3LYP functional,[11] where the HOMO is predicted to derive from a bonding combination of two s orbitals, sσ_g. Experimental spectroscopic studies on Cu_2 and Au_2[50−54] also assumed the (sσ_g^2)(sσ_u*^{0}) electronic configuration because this is consistent with $^1\Sigma_u^+$(sσ_g→sσ_u*) as the first singlet excited state. Nevertheless, most recent spectroscopic studies[51−54] actually reveal that for both Cu_2 and Au_2 the two lowest excited states, A and B, of 0_u^+ symmetry are strongly spin−orbit coupled and derive from $^1\Sigma_u^+$(sσ_g→sσ_u*) and $^3\Pi_u$(dπ_g→sσ_u*) states corroborating our expectation that valence s and d levels lie rather close and are able to mix via either spin−orbit interaction or s-d hybridization. In our calculations the energy difference between the sσ_g and dσ_u* (HOMO) orbitals of Cu_2 was determined to be just 0.3 eV, i.e., much smaller than the whole span of Cu 3d orbitals, 1.63 eV. Whether or not the dσ_u* orbital is the correct HOMO actually does not affect the qualitative pattern of optical transitions of dimers in the gas phase as all low-lying d → s transitions have zero or vanishing intensity in our TDDFT approach, where spin−orbit coupling is not included (Table 3). For the same reason all singlet−triplet transitions in our calculations are spin-forbidden and have zero intensity. Our calculated values for sσ_g → sσ_u* transitions for Cu_2 and Au_2 (2.53 and 2.76 eV) are slightly lower than the experimental X → B excitation energies, 2.69 eV for Cu_2[52] and 3.18 eV for Au_2.[53] (The B state has more $^1\Sigma_u^+$ character than the A state.) The X → A excitation energies, 2.53 eV for Cu_2[50] and 1.76 eV

TABLE 2: Calculated Vertical Transition Energies (eV) and Oscillator Strengths (in Square Brackets) of the Main Low-Lying Excitations for Coinage Metal Atoms Supported at F_s^+ and F_s Sites of MgO(001)[a]

	M at F_s^+			M at F_s		
	$ns \rightarrow F_s$	$ns \rightarrow np_{x,y}$[b]	$(n-1)d \rightarrow np_{x,y}$	$F_s \rightarrow np_{x,y}$[b]	$F_s \rightarrow np_z$	$F_s \rightarrow (n+1)p_{x,y}$[b]
Cu	3.28 (A_1) [0.081]	3.80 (E) [0.052]	3.86−5.59, 4.37 (E) [0.066][c]	0.72 (E) [0.007]	1.35 (A_1) [0.081]	1.78 (E) [0.033]
Ag	3.30 (A_1) [0.161]	3.88 (E) [0.122]	4.22−6.64, 4.41 (A_1) [0.070][c]	0.86 (E) [0.009]	1.48 (A_1) [0.096]	1.81 (E) [0.016]
Au	3.68 (A_1) [0.055]	4.21 (E) [0.043]	4.24−6.56, 4.36 (A_1) [0.058][c]	0.93 (E) [0.002]	1.52 (A_1) [0.056]	1.83 (E) [0.009]

[a] Adsorbed atoms were calculated in C_{4v} symmetry. The irreducible representations given in parentheses characterize the transition dipole moment. [b] For transitions of E symmetry, oscillator strengths are given per partner. [c] Transition with maximum intensity.

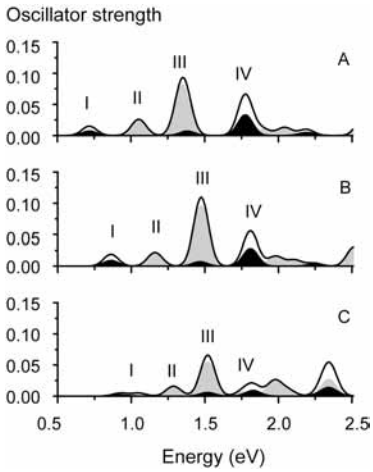

Figure 5. Absorption spectra of coinage metal atoms Cu (A), Ag (B), and Au (C) adsorbed at an F_s site of the MgO(001) surface. Polarization-resolved spectra are indicated by shading; layout is as in Figure 1. See the text for a discussion of the major peaks marked with I, II, III, and IV.

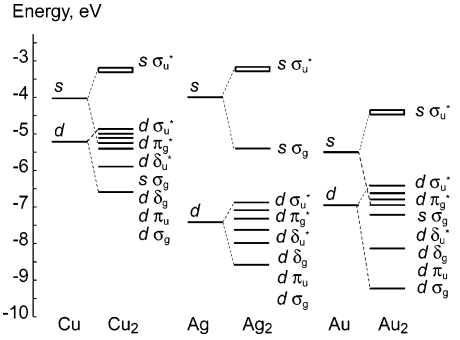

Figure 6. Frontier molecular orbital levels of dimers Cu_2, Ag_2, and Au_2 in the gas phase, obtained with an all-electron BP86 calculation. The LUMO $s\sigma_u^*$ is indicated by an open horizontal bar.

for Au_2,[53] are lower than our theoretical values. A TDDFT calculation[11] using the hybrid B3LYP approach yielded a value of 2.89 eV for the $s\sigma_g \rightarrow s\sigma_u^*$ transition in Cu_2. That study reported only the lowest $d \rightarrow s$ excitation energies, beginning at 2.53 eV, which is notably higher than our result, 1.90 eV. We attribute this difference to the use of a different xc functional, B3LYP,[11] which affects the MO ordering (see above) and, in general, increases the HOMO−LUMO gap. That previous study[11] did not report transitions of the $d \rightarrow p$ type.

For Ag_2, we find the same HOMO and LUMO, $s\sigma_g$ and $s\sigma_u$, as inferred from MRD-CI ground and excited states and underlying HF MOs[55] and also supported by spectroscopic measurements.[56] This difference to Cu_2 and Au_2 is clearly a consequence of a larger separation between the valence s and d levels in Ag (Figure 6).

The first transition of Ag_2 with nonzero intensity is the HOMO−LUMO transition of $s \rightarrow s$ nature corresponding to X $^1\Sigma_g^+ \rightarrow {}^1\Sigma_u^+(s\sigma_g \rightarrow s\sigma_u^*)$, just as calculated in the case of Cu_2 and Au_2. The experimental value for this excitation energy of Ag_2 is 2.85 eV,[56] 0.2 eV lower than our result, 3.05 eV. According to the present calculations, the first $d \rightarrow s$ transition with intensity appears at 5.41 eV ($d\sigma_g \rightarrow s\sigma_u^*$). This value is very close to the adiabatic transition energy 5.55 eV determined for the corresponding $X^1\Sigma^+_g \rightarrow 2^1\Sigma^+_u$ transition calculated with a MRD-CI method.[55]

For dimers adsorbed at regular sites of MgO, the MO order does not change significantly as the interaction with the MgO surface is mainly of polarization type. From our earlier study,[21] the adsorption energies of Cu_2, Ag_2, and Au_2 in the most favorable upright orientation are 132, 80, and 164 kJ mol^{-1}, respectively. The nature of HOMO and LUMO remains the same as for M_2 species in the gas phase. Thus, in dimers adsorbed at O^{2-} sites of ideal MgO(001) the lowest transitions are of the type HOMO → LUMO, i.e., $d\sigma_u^* \rightarrow s\sigma_u^*$ for Cu_2 and Au_2 (labeled I in Figure 7), and $s\sigma_g \rightarrow s\sigma_u^*$ for Ag_2 (labeled II). Here, we preserved the notations used for MOs of diatomics in the gas phase, although the symmetry in the adsorbed systems has been lowered to C_s and thus previously forbidden transitions $\sigma_u^* \rightarrow \sigma_u^*$ have become allowed via interaction with the support. Furthermore, note that for Cu_2 and especially for Au_2 s-d hybridization becomes even more pronounced than in the corresponding molecules in the gas phase, which permits a certain degree of mixing between $d\sigma_u^*$ and $s\sigma_g$ MOs. For the three coinage metal diatomics under study, the calculated absorption spectra exhibit quite different spectral shape and types of transitions (Figure 7).

For Cu_2, the first two peaks at 2.6 and 3.6 eV correspond to the transitions $d\sigma_u^* \rightarrow s\sigma_u^*$ (I) and $s\sigma_g \rightarrow s\sigma_u^*$ (II). Both transitions blue shift by ∼1 eV relative to those calculated for free Cu_2 (Table 3). This result is at variance with findings of Del Vitto et al.[11] who reported an almost unchanged transition energy for the $s\sigma_g \rightarrow s\sigma_u^*$ excitation upon adsorption, 2.95 eV, vs 2.89 eV in the gas phase. The low-intensity feature at 4.0 eV in Figure 7 is assigned as $s\sigma_g \rightarrow p\pi_u$ (III) followed by $d\sigma_u^* \rightarrow p\pi_u$ at 4.1 eV. Beyond that point the continuum of the support sets and thus makes further identification of transitions within the metal particle difficult. As already pointed out, this much too early emergence of the continuum is a shortcoming of the xc approximation used in the present TD−DFT study.

Transitions of adsorbed Ag_2 begin at 3.1 eV with an intense $s\sigma_g \rightarrow s\sigma_u^*$ peak followed by another intense transition at 3.8 eV of $s\sigma_g \rightarrow p\pi_u$ type (III). The $s\sigma_g \rightarrow s\sigma_u^*$ transition remains at about the same energy as in the gas-phase dimer (3.05 eV), consistent with the essentially unchanged HOMO−LUMO gap, ∼2 eV in adsorbed Ag_2. We note the difference to Cu_2 and Au_2; in the latter species, the HOMO−LUMO gap increased by up to 1 eV upon adsorption, indicative of a favorable

TABLE 3: Calculated Vertical Transition Energies (eV) and Oscillator Strengths (in Square Brackets) for Coinage Metal Dimers, in the Gas Phase (gp) and Supported at O^{2-} Sites of MgO(001)[a]

		d → s[b]		s → s		d → p and s → p[c]	
	system	transition	character	transition	character	transition	character
Cu_2	gp	1.90 [0.000]	$\sigma_u^* \rightarrow \sigma_u^*$	2.53 [0.080]	$\sigma_g \rightarrow \sigma_u^*$	3.45−5.43	
		1.91 [0.006]	$\pi_g^* \rightarrow \sigma_u^*$			3.67 [0.016]	$d\pi_g^* \rightarrow \pi_u$
		2.07 [0.000]	$\delta_u^* \rightarrow \sigma_u^*$			4.19 [0.036]	$d\delta_g \rightarrow \pi_u$
		2.30 [0.000]	$\delta_g \rightarrow \sigma_u^*$			4.26 [0.063]	$d\sigma_u^* \rightarrow \sigma_g$
		2.81 [0.000]	$\pi_u \rightarrow \sigma_u^*$			5.32 [0.007]	$d\pi_u \rightarrow \sigma_g$
		4.79 [0.531]	$\sigma_g \rightarrow \sigma_u^*$			5.43 [0.038]	$d\sigma_g \rightarrow \pi_u$
						4.54 [0.389]	$s\sigma_g \rightarrow \pi_u$
	O^{2-} site	2.12−6.44	$\sigma_u^* \rightarrow \sigma_u^*$	3.55 [0.094]	$\sigma_g \rightarrow \sigma_u^*$	3.99 [0.003]	$d\sigma_u^* \rightarrow \sigma_g$
		2.60 [0.045][d]	$\sigma_g \rightarrow \sigma_u^*$			4.09 [0.032]	$d\sigma_u^* \rightarrow \pi_u$
		4.26 [0.046][d]				4.09 [0.003]	$d\sigma_u^* \rightarrow \pi_u$
						3.96 [0.033]	$s\sigma_g \rightarrow \pi_u$
						3.96 [0.012]	$s\sigma_g \rightarrow \pi_u$
Ag_2	gp	3.71 [0.000]	$\sigma_u^* \rightarrow \sigma_u^*$	3.05 [0.367]	$\sigma_g \rightarrow \sigma_u^*$	3.70−7.96	
		3.83 [0.004]	$\pi_g^* \rightarrow \sigma_u^*$			6.01 [0.054]	$d\pi_g^* \rightarrow \pi_u$
		4.03 [0.000]	$\delta_u^* \rightarrow \sigma_u^*$			6.43 [0.419]	$d\sigma_u^* \rightarrow \sigma_g$
		4.23 [0.000]	$\delta_g \rightarrow \sigma_u^*$			6.47 [0.218]	$d\delta_g \rightarrow \pi_u$
		4.79 [0.000]	$\pi_u \rightarrow \sigma_u^*$			7.30 [0.046]	$d\sigma_g \rightarrow \pi_u$
		5.41 [0.060]	$\sigma_g \rightarrow \sigma_u^*$			7.37 [0.050]	$d\pi_u \rightarrow \sigma_g$
						4.70 [0.754]	$s\sigma_g \rightarrow \pi_u$
	O^{2-} site	3.30−5.86	$\sigma_u^* \rightarrow \sigma_u^*$	3.12 [0.502]	$\sigma_g \rightarrow \sigma_u^*$	4.28 [0.004]	$d\sigma_u^* \rightarrow \sigma_g$
		4.54 [0.041][d]				3.81 [0.117]	$s\sigma_g \rightarrow \pi_u$
						3.87 [0.131]	$s\sigma_g \rightarrow \pi_u$
Au_2	gp	2.27 [0.000]	$\sigma_u^* \rightarrow \sigma_u^*$	2.76 [0.122]	$\sigma_g \rightarrow \sigma_u^*$	5.05−8.13	
		2.33 [0.011]	$\pi_g^* \rightarrow \sigma_u^*$			5.23 [0.003]	$d\pi_g^* \rightarrow \pi_u$
		2.40 [0.000]	$\delta_u^* \rightarrow \sigma_u^*$			5.50 [0.014]	$d\sigma_u^* \rightarrow \sigma_g$
		2.73 [0.000]	$\delta_g \rightarrow \sigma_u^*$			6.07 [0.288]	$d\delta_g \rightarrow \pi_u$
		3.84 [0.000]	$\pi_u \rightarrow \sigma_u^*$			7.71 [0.363]	$d\pi_u \rightarrow \sigma_g$
		6.35 [0.804]	$\sigma_g \rightarrow \sigma_u^*$			8.13 [0.170]	$d\sigma_g \rightarrow \pi_u$
						5.62 [0.288]	$s\sigma_g \rightarrow \pi_u$
	O^{2-} site	2.93−5.53	$\sigma_u^* \rightarrow \sigma_u^*$	4.01 [0.006]	$\sigma_g \rightarrow \sigma_u^*$	4.91 [0.003]	$d\sigma_u^* \rightarrow \sigma_g$
		3.02 [0.052][d]				4.17 [0.004]	$d\sigma_u^* \rightarrow \pi_u$
						4.18 [0.005]	$d\sigma_u^* \rightarrow \pi_u$

[a] MO symmetries are given for the point group $D_{\infty h}$. For M_2 adsorbed on MgO, the same notations are used to show correspondence between the MOs of gas-phase and adsorbed molecules. [b] For degenerate transitions, oscillator strengths are given per partner. [c] Only transitions with nonzero intensity are listed; for adsorbed species, the range up to 4.5 eV is considered. [d] Transition with maximum intensity.

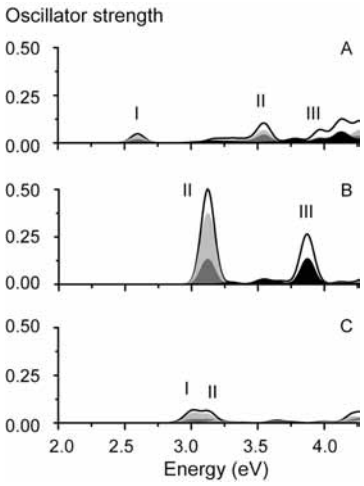

Figure 7. Absorption spectra of coinage metal dimers Cu_2 (A), Ag_2 (B), and Au_2 (C) adsorbed at an O^{2-} site of a defect-free MgO(001) surface. Polarization-resolved spectra are indicated by shading: dark gray, *x*-polarized transitions; black, *y*-polarized transitions; light gray, *z*-polarized transitions. See the text for a discussion of the major peaks marked with I, II, and III.

interaction with the MgO support. This is also reflected in 1.6 and 2 times higher adsorption energies of Cu_2 and Au_2 compared to Ag_2.

For Au_2, the first transitions with intensity appear at 3.0 eV with the weak $d\sigma_u^* \rightarrow s\sigma_u^*$ band and remain at rather low intensity in the considered energy range up to 4.25 eV (Figure 7). The $d\sigma_u^* \rightarrow s\sigma_u^*$ transition lies 0.7 eV above the gas-phase value, 2.26 eV; this upward shift is of similar magnitude as determined for Cu_2 (Table 3).

Although quite different looking, the three spectra can be characterized by some common features. In the considered energy range, the two main transitions are of type $d\sigma_u^* \rightarrow s\sigma_u^*$ (I) and $s\sigma_g \rightarrow s\sigma_u^*$ (II) (Figure 7). The remarkably high intensity of the latter transition in case of Ag_2 can probably be explained by the relatively pure $s\sigma_g$ character of the HOMO, separated by 0.8 eV from the underling d-manifold, and the weak interaction with the support, whereas for Cu_2 and Au_2, $s\sigma_g$ and $d\sigma_u^*$ mixing is quite pronounced. The former transition, of $d\sigma_u^* \rightarrow s\sigma_u^*$ type, is less intense because it is parity forbidden for dimers in the gas phase. Furthermore, the d → s transitions are dipole forbidden in the free atoms.

Inclusion of SO interaction is expected to affect the calculated spectra at least of Au_2, because of an upward spread in energy of the d-manifold and thus a decreased HOMO−LUMO gap (by ∼0.5 eV as revealed by our test calculations for the gas-phase dimer).

Dimers at F_s^+ and F_s Vacancy Sites. Coinage metal dimers adsorb at vacancy sites in an almost upright orientation with some degree of tilting with respect to the surface normal.[21] The bonding involves, as shown above for atoms, considerable shifts of the valence (frontier) orbitals and a change of the electronic configuration of the adsorbed metal species. To first approximation, the MO picture of bonding can be described as interaction of the singly (or doubly) occupied vacancy level F_s and the $s\sigma_u^*$ LUMO of the dimer. As a result, the bonding combination $s\sigma_u^* + F_s$ is lowered in energy and the antibonding combination

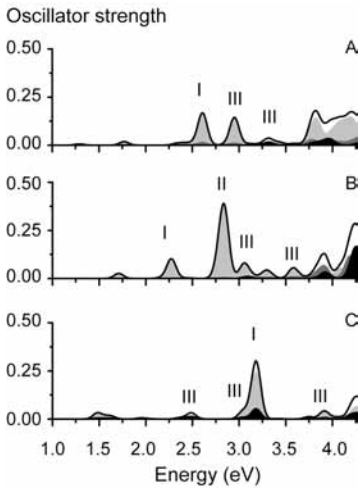

Figure 8. Absorption spectra of coinage metal dimers Cu_2 (A), Ag_2 (B), and Au_2 (C) adsorbed at an F_s^+ site of the MgO(001) surface. Layout is as in Figure 7. See the text for a discussion of the major peaks marked with I, II, and III.

$s\sigma_u^*-F_s$ shifts upward, close to the (bonding) virtual MOs $p\sigma_g$ and $p\pi_u$ of M_2, while mixing considerably with $p\sigma_g$. For simplicity, in the following we will refer to the two MOs with a contribution from the cavity as $s\sigma_u^*$ and F_s instead of $s\sigma_u^*+F_s$ and $s\sigma_u^*-F_s$. Note, however, that due to interaction with the support, there are several unoccupied levels with mixed F_s and $p\sigma_g$ character; thus, our simplified labeling of virtual orbitals is just a convenience. The adsorption interaction just described stabilizes the electron from the vacancy level F_s^+ at the lowered $s\sigma_u^*$ orbital. However, there is also a destabilizing effect due to the weakening of the M−M bond, yet the former contribution seems to dominate as adsorption energies of M_2 at F_s^+ (66, 64, and 116 (kJ mol^{-1})/atom for Cu_2, Ag_2, and Au_2, respectively) are equal or greater than for diatomics adsorbed at regular O^{2-} sites (66, 40, and 82 kJ mol^{-1}/atom).[21] The strongest increase in the binding energy, for Au_2, correlates with the largest downward shift of $s\sigma_u^*$ (almost 1 eV below the corresponding MOs of Cu_2 and Ag_2).

The bonding picture at neutral vacancy sites is quite similar, only that the HOMO $s\sigma_u^*+F_s$ acquires a second electron from the vacancy site. The net stabilizing effect is even stronger on F_s than on F_s^+ as the vacancy orbital is doubly occupied. The adsorption interaction on a neutral F_s site is 60−70% stronger for all three dimers than on a charged defect site F_s^+ and 1.6−2.7 times larger than at regular O^{2-} sites.[21]

The spectral features of diatomics adsorbed at vacancy sites are consistent with the orbital pattern just described. For dimers adsorbed at F_s^+ (Figure 8), the first relatively strong transition is $s\sigma_u^* \rightarrow p\sigma_g$ (I), which appears at 2.61, 2.27, and 3.18 eV for Cu_2, Ag_2, and Au_2, respectively (Table 4). The highest energy of this transition is calculated for Au_2, again consistent with the largest downward shift of $s\sigma_u^*$ and the strongest binding to the surface as mentioned above. The low-intensity peaks to the left of I (Figure 8) are mainly from the higher occupied d orbitals to $s\sigma_u^*$ (and $s\sigma_g \rightarrow s\sigma_u^*$ in case of Ag_2). For Ag_2, the next well-pronounced high-intensity peak (II) corresponds to the transition $s\sigma_u^* \rightarrow p\pi_g$. In fact, the MO to that we refer as $p\pi_g$ is its A′ component, which bears a sizable contribution from F_s and also mixes strongly with $p\sigma_g$ due to a considerable tilting of Ag_2 with respect to the surface normal, 29°.[21] Transitions of this type are found to appear with much lower intensity for Cu_2 and Au_2 (Table 4). One reason for that difference could be a less significant tilting of Cu_2 and Au_2 moieties, at most 10°.

TABLE 4: Calculated Vertical Transition Energies (eV) and Oscillator Strengths (in Square Brackets) for Coinage Metal Dimers Supported at F_s^+ and F_s Sites of MgO(001)[a]

	system	$s\sigma_u^* \rightarrow p\sigma_g$	$s\sigma_u^* \rightarrow p\pi_u$[b]	$s\sigma_u^* \rightarrow F_s$
Cu_2	F_s^+ site	2.61 [0.133]	3.91 [0.012]	3.36 [0.003]
			3.92 [0.011]	
	F_s site	2.17 [0.123]	2.46 [0.006]	2.54 [0.082]
			2.46 [0.009]	
Ag_2	F_s^+ site	2.27 [0.082]	2.84 [0.281]	3.29 [0.028]
			2.84 [0.000]	
	F_s site	2.08 [0.142]	2.12 [0.001]	2.48 [0.096]
			2.13 [0.001]	
Au_2	F_s^+ site	3.17 [0.220]	3.15 [0.011]	3.97 [0.002]
			3.17 [0.006]	
	F_s site	2.72 [0.122]	2.78 [0.000]	3.09 [0.099]
			2.78 [0.000]	

[a] MO symmetries are given for the point group $D_{\infty h}$ to show the correspondence between MOs of gas-phase and adsorbed molecules. [b] For degenerate transitions, oscillator strengths are given per partner.

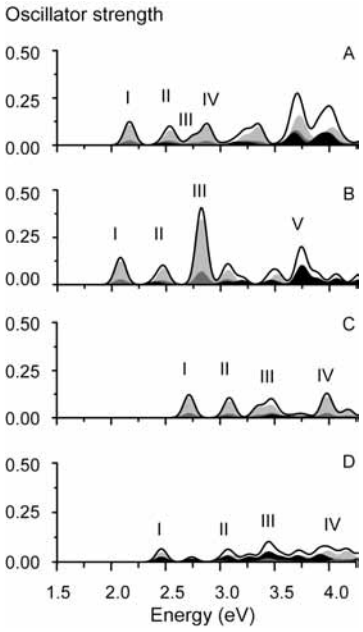

Figure 9. Absorption spectra of coinage metal dimers Cu_2 (A), Ag_2 (B), Au_2 in "upright" orientation (C), and Au_2 in "tilted" orientation (D), adsorbed at an F_s site of the MgO(001) surface. Layout is as in Figure 7. See the text for a discussion of the major peaks marked with I−V.

However, we will see in the following that the same strong peak appears for Ag_2 (but not for Cu_2 and Au_2) at a neutral F_s defect where only a minor tilting was calculated for all three dimers. This anomalous behavior of Ag_2 may be due to its weaker interaction with the MgO surface. Thus, low-lying transitions have more pronounced intramolecular character, whereas Cu_2 and Au_2 interact stronger with the support, which results in many mixed states and a distribution of oscillator strength over a range of transitions. Transitions from $s\sigma_u^*$ to F_s carry very low intensity (Table 4). Only for Ag_2 is this transition at 3.3 eV calculated to be visible in the spectrum. Other well-separated peaks to the right of I (and also to the left of I in case of Au_2), marked as III in Figure 8, are assigned as $d \rightarrow s\sigma_u^*$.

Absorption spectra of dimers supported at neutral vacancy sites F_s of the MgO(001) surface (Figure 9, Table 4) can be interrelated with those for M_2 at the corresponding F_s^+ sites. As stated above, the qualitative frontier orbital picture differs only by the doubly occupied $s\sigma_u^*$ HOMO level instead of the singly occupied level of dimers adsorbed at F_s^+. In the spectra

of all three coinage metal dimers, the first peaks of high intensity (I) again correspond to the $s\sigma_u^* \rightarrow p\sigma_g$ transition. At neutral vacancy sites, these transitions are calculated 0.2−0.5 eV lower in energy compared to the spectra of dimers at charged defect sites F_s^+. The $s\sigma_u^* \rightarrow F_s$ transitions (II) follow with comparable intensities at 2.5, 2.4, and 3.1 eV for Cu_2, Ag_2, and Au_2, respectively. The next higher band (III) that appears in all three spectra is also of $s\sigma_u^* \rightarrow p\sigma_g$ type, but it involves a higher lying orbital of partial $p\sigma_g$ character. In the case of Ag_2, transitions II and III cannot be unambiguously separated because both are actually mixtures involving large contributions of $s\sigma_u^* \rightarrow F_s$ and $s\sigma_u^* \rightarrow p\sigma_g$. Other identifiable higher transitions (IV) are from the top of the d manifold, $d\sigma_u^* \rightarrow F_s$, found in the spectra of Cu_2 and Au_2 around 2.9 and 4.0 eV, respectively; for Ag_2 they are not observed in the considered energy range as occupied d orbitals lie quite low in energy. Instead, a $s\sigma_g \rightarrow p\pi_g$ transition (V) with sizable intensity is found around 3.7 eV. Unmarked bands involve transitions to higher lying orbitals with considerable admixtures of MgO levels. Overall, the spectral shapes of the three congeners differ notably (Figure 9). Still the transition $s\sigma_u^* \rightarrow p\sigma_g$ can be considered characteristic, ordered in energy according to $Ag_2 < Cu_2 < Au_2$; that pattern is similar to what was calculated for the coinage metal dimers adsorbed at F_s^+ (Figure 8).

Optical transitions of Au_2 at F_s centers of MgO(001) have previously been studied computationally[12] using TDDFT in the LDA approximation. In that work, two almost isoenergetic minima were reported, one with the gold dimer standing "upright" and another one with the dimer tilted by 33° from the surface normal. Surprisingly, calculations yielded completely different spectral shapes for the two isomers, despite only a slight difference in geometry. Although we determined only one minimum (the upright geometry) for this system,[21] the remarkable similarity of our predicted spectrum (Figure 9C) to that for a tilted geometry in ref 12 motivated us to calculate also the optical transitions for a tilted gold dimer. We used the same tilt angle as reported in ref 12, 33°, but kept the Au−Au distance as previously optimized with our embedded cluster model approach, at 2.63 Å. This calculation revealed only a slight shift (at most 0.3 eV) of the main bands I−IV with respect to those of the "upright" structure, although oscillator strengths decreased on the whole and migrated partially from the *z* to the *y* spectral component (following the dimer axis tilted in the *y*-direction), and several previously forbidden transitions appeared with low intensity (Figure 9D). The general agreement with the spectrum of the tilted isomer in ref 12 may seem worsened due to appearance of several low-intensity transitions; however, the positions of the main bands still agree within 0.1−0.2 eV. Our test showed a relatively small variation in the spectral shape upon changing the orientation of Au_2 with respect to MgO surface from an essentially upright to the titled geometry, at variance with predictions of ref 12. Thus, the apparently good agreement of our spectrum for the "upright" structure (Figure 9C) with the TDLDA spectrum of a tilted dimer[12] seems to be coincidental.

3.3. Effect of Cluster Embedding on Calculated Optical Properties. Finally, we address the importance of proper cluster embedding for accurate calculations of vertical excitation energies and oscillator strengths. To this end, we compared three cluster models, using a Cu atom supported at a regular O^{2-} site of the ideal MgO(001) surface as benchmark system. Model I is our standard EPE model, briefly described in the section *Computational Methods* and in more detail elsewhere.[35] In model II, the QM cluster environment was kept untouched, but the representation of the long-range electrostatic potential was removed. In other words, the surface charge representation of the electrostatic embedding potential (SCREEP), which accounts for the electrostatic field due to the distant part of the infinite crystal, was eliminated, but a point-charge array of 644 point charges representing the electrostatic field of the nearby region of the support (region II of EPE[35]) was kept. Model III comprised only the QM cluster model $CuMg_9O_9$ without any embedding. The TDDFT results of these three models are compared in Table 5.

TABLE 5: Vertical Transition Energies (eV) and Oscillator Strengths (in Square Brackets) for Supported Cu Atom at O^{2-} Sites of MgO(001) with Three Cluster Models of the Support[a]

	calc		
model[a]	$(n-1)d \rightarrow ns$[b]	$ns \rightarrow np$[b]	$ns \rightarrow (n+1)s$
I	2.13 (E) [0.001]	2.45 (E) [0.072]	3.41 (A_1) [0.076]
	2.20 (A_1) [0.000]	2.86 (A_1) [0.004]	
	2.36 (B_2) [0.000]		
	2.39 (B_1) [0.000]		
II	2.14 (E) [0.001]	2.46 (E) [0.063]	3.08 (A_1) [0.043]
	2.20 (A_1) [0.000]	2.11 (A_1) [0.002]	
	2.36 (B_2) [0.000]		
	2.39 (B_1) [0.000]		
III	1.45 (E) [0.010]	0.85 (E) [0.049]	3.10 (A_1) [0.036]
	1.68 (A_1) [0.000]	0.92 (A_1) [0.080]	
	1.69 (B_2) [0.000]		
	1.85 (B_1) [0.000]		

[a] I: $Mg_9O_9(Mg^{PP})_{16}$ cluster embedded in an elastic polarizable environment (EPE). II: same as I, i.e., with an array of 644 point charges representing the electrostatic field of the nearby region of the support, but without the surface charge representation of the electrostatic embedding potential (SCREEP). III: Mg_9O_9 model without embedding. [b] For degenerate transitions, oscillator strengths are given per partner.

The $d \rightarrow s$ transition energies and the corresponding oscillator strengths, calculated in model II, agree quantitatively with the benchmark values of model I, whereas the $s \rightarrow p$ and $s \rightarrow s$ transitions are shifted by 0.3−0.7 eV. However, the average deviation in transition energies can be considered small (<0.3 eV) and the maximum deviation obtained was 0.7 eV. The oscillator strengths deviated at most 0.06 and on average by 0.01 from those obtained with model I. Model III underestimates the $d \rightarrow s$ transition energies by 0.5−0.7 eV and particularly strongly the $s \rightarrow p$ transition energies, by 1.6−2.0 eV. Although the $s \rightarrow s$ transition energies predicted by model III closely match those calculated with Model II, this is probably fortuitous because the average deviation of transition energies from model I, calculated for the 30 lowest transitions, was 0.8 eV and the maximum deviation was 2.6 eV. These results illustrate the fact that model III is too crude to be useful.

This simple test substantiates the importance of cluster embedding, which affects the ordering of the MOs and hence the excitation energies calculated with a TDDFT method. Inclusion of the SCREEP, however, overall contributes only little, in particular when one considers the overall predictive accuracy of the approach used here, but omission may affect individual transitions too much to prevent correct assignment for some systems.

4. Conclusions

Calculating the energy spectrum of metal particles adsorbed at solid surfaces is a challenging task for wave function based quantum chemistry methods. Metal atoms and dimers chemisorbed on the surface of ionic MgO not only are affected by

the strong electrostatic field and repulsive exchange interactions with oxygen anions on the surface but also undergo substantial rearrangements in the electronic structure of the frontier orbitals when interacting with point-defect sites, such as oxygen vacancy sites. Hybrid quantum mechanical/molecular mechanical cluster models featuring a suitable representation of the ionic crystalline environment can be treated by linear response TDDFT and thus provide a cost-effective predictive approach to the energetics and the optical spectrum of adsorbed metal species.

We have studied systematically absorption spectra of coinage metal atoms and diatomics supported on MgO(001) terraces at regular O^{2-} sites as well as neutral and charged oxygen vacancies (F_s and F_s^+) using an accurate (scalar-relativistic where necessary) all-electron DF method in combination with cluster embedding in an elastic polarizable environment. We calculated energies and oscillator strengths of vertical electronic transitions within the framework of linear response time-dependent density functional theory using the BP86 xc potential and all-electron basis sets. We have investigated (i) to what extent interaction with the support affects the optical properties compared to the species in the gas phase, (ii) how spectral signatures of species adsorbed at regular and vacancy sites differ from each other, (iii) trends among congeners, and (iv) how important embedding is for accurate predictions of excitation energies of adsorbed systems.

We have simulated absorption spectra for excitation energies up to 4−4.5 eV and discussed the nature of allowed transitions in detail. Interaction with MgO support even at regular O^{2-} sites, where binding is dominated by electrostatic polarization, perturbs significantly the atomic or molecular orbitals; therefore, transition energies shift by up to 2−2.5 eV compared to gas-phase references. Hence, relying on gas-phase data while assigning optical spectra of supported species may not be meaningful. Interaction with F_s and F_s^+ sites results in more drastic changes of the frontier MO picture. A notable delocalization of the occupied frontier orbital into the charged defect cavity contributes substantially to its stabilization. Thus, nature and sequence of major transitions changes significantly on going from regular to defect sites. The optical spectra of atoms and dimers at regular O^{2-} sites are dominated by internal excitations; in contrast, the trapped state of the vacancy site plays a prominent role in determining spectra of atoms and dimers adsorbed at defect sites. We identified the most intense low-energy features of all spectra as excitations to particle-hole states that involve frontier orbitals of the adsorbed species and, eventually, the vacancy level of the trapped electron(s). Knowledge of the qualitative pattern of these transitions should help in the assignment of experimental spectra of these systems.

Comparison of the three coinage metals shows in general similar characters of the transitions, although they differ energetically and by relative intensities. Particularly for adsorbed Au atoms and dimers, the lowest transitions with intensity are typically blue-shifted with respect to the spectra of the other two congeners. We rationalized these shifts as relativistic effects, e.g., shifts of orbitals with dominant Au 6s contributions to lower energies and a widening of the HOMO−LUMO gap in adsorption complexes of Au and Au_2. Analogous Cu and Au species resemble each other in many cases due to closely lying s and d levels, which interact and hybridize, whereas d-levels of Ag complexes are more localized and not directly involved in bonding.

Finally, we point to the model character of the present study. In this context, recall that spin−orbit interaction was not included in our (scalar) relativistic treatment of systems comprising Ag and Au atoms. For systems with heavy elements, application of a more sophisticated TDDFT method[57] seems advantageous to explore the effect of spin−orbit interaction on hole states with substantial d-character.

Acknowledgment. L.V.M. expresses her deep gratitude to her Ph.D. advisor Prof. M. C. Lin for his past and present support and his invaluable influence on her scientific career. We thank Prof. K. M. Neyman and Dr. C. Inntam for their valuable help during the initial stage of this work. This work was supported by Deutsche Forschungsgemeinschaft and Fonds der Chemischen Industrie (Germany).

References and Notes

(1) Peyser, L. A.; Vinson, A. E.; Bartko, A. P.; Dickson, R. M. *Science* **2001**, *291*, 103−106.

(2) Kreibig, U.; Vollmer, M. *Optical Properties of Metal Clusters*; Springer: Berlin, 1995.

(3) Mayer, C.; Palkovits, R.; Bauer, G.; Schalkhammer, T. *J. Nanoparticle Res.* **2001**, *3*, 361−371.

(4) Haruta, M.; Yamada, N.; Kobayashi, T.; Iijima, S. *J. Catal.* **1989**, *115*, 301−309.

(5) (a) Rösch, N.; Vayssilov, G. N.; Neyman, K. M. In *Host/Guest Systems Based on Nanoporous Crystals*; Laeri, F.; Schüth, F.; Simon, U.; Wark, M., Eds.; Wiley-VCH: Weinheim, 2003, p. 339−350. (b) Rösch, N.; Nasluzov, V. A.; Neyman, K. M.; Pacchioni, G.; Vayssilov, G. N. In *Computational Material Science*; Leszczynski, J. Ed.; Theoretical and Computational Chemistry Series; Elsevier: Amsterdam, 2004; Vol. 15, p. 367−450. (c) Neyman, K. M.; Vayssilov, G. N.; Rösch, N. *J. Organomet. Chem.* **2004**, *689*, 4384−4394.

(6) Guzman, J.; Gates, B. C. *Dalton Trans.* **2003**, 3303−3318.

(7) Pacchioni, G. In *Nanocatalysis*; Heiz, U.; Landman, U., Eds.; Springer: Berlin, 2007, p. 103−243.

(8) (a) Heiz, U.; Schneider, W.-D. *J. Phys. D* **2000**, *33*, R85−R102. (b) *Nanocatalysis*; Heiz, U.; Landman, U., Eds.; Springer: Berlin, 2007.

(9) (a) Di Valentin, C.; Scagnelli, A.; Pacchioni, G.; Risse, Th.; Freund, H.-J. *Surf. Sci.* **2006**, *600*, 2434−2442. (b) Yulikov, M.; Sterrer, M.; Heyde, M.; Rust, H.-P.; Risse, Th.; Freund, H.-J.; Pacchioni, G.; Scagnelli, A. *Phys. Rev. Lett.* **2006**, *96*, 146804, 1−4.

(10) Kohl, C.; Calvayrac, F.; Reinhard, P.-G.; Suraud, E. *Surf. Sci.* **1998**, *405*, 74−86.

(11) Del Vitto, A.; Sousa, C.; Illas, F.; Pacchioni, G. *J. Chem. Phys.* **2004**, *121*, 7457−7466.

(12) Walter, M.; Häkkinen, H. *Phys. Rev. B* **2005**, *72*, 205440, 1−5.

(13) Antonietti, J.-M.; Michalski, M.; Heiz, U.; Jones, H.; Lim, K. H.; Rösch, N.; Del Vitto, A.; Pacchioni, G. *Phys. Rev. Lett.* **2005**, *94*, 213402, 1−4.

(14) Del Vitto, A.; Pacchioni, G.; Lim, K. H.; Rösch, N.; Antonietti, J.-M.; Michalski, M.; Heiz, U.; Jones, J. *J. Phys. Chem. B* **2005**, *109*, 19876−19884.

(15) Wilcoxon, J. P.; Abrams, B. L. *Chem. Soc. Rev.* **2006**, *35*, 1162−1194.

(16) Hutter, E.; Fendler, J. H. *Adv. Mater.* **2004**, *16*, 1685−1706.

(17) Gilb, S.; Jacobson, K.; Schooss, D.; Furche, F.; Ahlrichs, R.; Kappes, M. M. *J. Chem. Phys.* **2004**, *121*, 4619−4627.

(18) (a) Runge, E.; Gross, E. K. U. *Phys. Rev. Lett.* **1984**, *52*, 997−1000. (b) Casida, M. E. In *Recent Developments and Applications of Modern Density Functional Theory*; Seminario, J. M., Ed.; Elsevier: Amsterdam, 1996, Vol. 4, p. 391−439. (c) *Time-Dependent Density Functional Theory*; Marques, M. A. L.; Ullrich, C. A.; Nogueira, F.; Rubio, A.; Burke, K.; Gross, E. K. U., Eds.; Lecture Notes in Physics; Springer: Berlin, 2006, Vol. 706.

(19) Neyman, K. M.; Inntam, C.; Nasluzov, V. A.; Kosarev, R.; Rösch, N. *Appl. Phys. A* **2004**, *78*, 823−828.

(20) Neyman, K. M.; Inntam, C.; Matveev, A. V.; Nasluzov, V. A.; Rösch, N. *J. Am. Chem. Soc.* **2005**, *127*, 11652−11660.

(21) Inntam, C.; Moskaleva, L. V.; Neyman, K. M.; Nasluzov, V. A.; Rösch, N. *Appl. Phys. A* **2006**, *82*, 181−189.

(22) Inntam, C.; Moskaleva, L. V.; Yudanov, I. V.; Neyman, K. M.; Rösch, N. *Chem. Phys. Lett.* **2006**, *417*, 515−520.

(23) Neyman, K. M.; Inntam, C.; Moskaleva, L. V.; Rösch, N. *Chem. Eur. J.* **2006**, *13*, 277−286.

(24) Belling, T.; Grauschopf, T.; Krüger, S.; Mayer, M.; Nörtemann, F.; Staufer, M.; Zenger, C.; Rösch, N. In *High Performance Scientific and Engineering Computing*; Bungartz, H.-J.; Durst, F.; Zenger, C., Eds.; Lecture Notes in Computational Science and Engineering; Springer: Heidelberg, 1999, Vol. 8, p. 441−455.

(25) Belling, T.; Grauschopf, T.; Krüger, S.; Nörtemann, F.; Staufer, M.; Mayer, M.; Nasluzov, V. A.; Birkenheuer, U.; Hu, A.; Matveev, A.

V.; Shor, A. M.; Fuchs-Rohr, M. S.; Neymann, K. M.; Ganzushin, D. I.; Kerdcharoen, T.; Woiterski, A.; Gordienko, A. B.; Majumder, S.; Rösch, N. ParaGauss, Version 3.1, Technische Universität München, **2004**.

(26) Dunlap, B. I.; Rösch, N. *Adv. Quant. Chem.* **1990**, *21*, 317−339.

(27) Becke, A. D. *Phys. Rev. A* **1988**, *38*, 3098−3100; Perdew, J. P. *Phys. Rev. B* **1986**, *33*, 8822−8824.

(28) (a) Häberlen, O. D.; Rösch, N. *Chem. Phys. Lett.* **1992**, *199*, 491−496. (b) Rösch, N.; Matveev, A. V.; Nasluzov, V. A.; Neyman, K. M.; Moskaleva, L. V.; Krüger, S. In *Relativistic Electronic Structure Theory − Applications*; Schwerdtfeger, P., Ed.; Theoretical and Computational Chemistry Series; Elsevier: Amsterdam 2004, Vol. 14, p. 656−722.

(29) (a) Görling, A.; Heinze, H. H.; Ruzankin, S. P.; Staufer, M.; Rösch, N. *J. Chem. Phys.* **1999**, *110*, 2785−2799. (b) Heinze, H. H.; Görling, A.; Rösch, N. *J. Chem. Phys.* **2000**, *113*, 2088−2099.

(30) Bosko, S. I. Dissertation, Technische Universität München: München 2007, in preparation.

(31) Matveev, A. V.; Mayer, M.; Rösch, N. *Comp. Phys. Comm.* **2004**, *160*, 91−119.

(32) (a) Wachters, A. J. *J. Chem. Phys.* **1970**, *52*, 1033−1036; Poirer, R.; Kari, R.; Csizimadia, I. G. *Handbook of Gaussian Basis Sets*; Elseivier: Amsterdam, 1985. (b) Hess, B. Private communication.

(33) Becke, A. D. *J. Chem. Phys.* **1988**, *88*, 2547−2553.

(34) Lebedev, V. I. *Sib. Math. J.* **1977**, *18*, 99−107.

(35) (a) Nasluzov, V. A.; Rivanenkov, V. V.; Gordienko, A. B.; Neyman, K. M.; Birkenheuer, U.; Rösch, N. *J. Chem. Phys.* **2001**, *115*, 8157−8171. (b) Nasluzov, V. A.; Rivanenkov, V. V.; Shor, A. M.; Neyman, K. M.; Birkenheuer, U.; Rösch, N. *Int. J. Quantum Chem.* **2002**, *90*, 386−402.

(36) (a) Yudanov, I.; Pacchioni, G.; Neyman, K. M.; Rösch, N. *J. Phys. Chem. B* **1997**, *101*, 2786−2792. (b) Neyman, K. M.; Vent, S.; Pacchioni, G.; Rösch, N. *Nuovo Cim. D* **1997**, *19*, 1743−1748. (c) Ferrari, A. M.; Xiao, C.; Neyman, K. M.; Pacchioni, G.; Rösch, N. *Phys. Chem. Chem. Phys.* **1999**, *1*, 4655−4661.

(37) (a) Musolino, V.; Selloni, A.; Car, R. *Phys. Rev. Lett.* **1999**, *83*, 3242−3245. (b) Bogicevic, A.; Jennison, D. R. *Surf. Sci.* **1999**, *437*, L741−L747. (c) Bogicevic, A.; Jennison, D. R. *Surf. Sci.* **2002**, *515*, L481−L486. (d) Coquet, R.; Hutchings, G. J.; Taylor, S. H.; Willock, D. J. *J. Mater. Chem.* **2006**, *16*, 1978−1988.

(38) Barnett, R.; Landman, U. *Phys. Rev. B* **1993**, *48*, 2081−2097.

(39) (a) Moore, C. E. *Atomic Energy Levels*; National Bureau of Standards Reference Data Series; U.S. GPO: Washington, DC, 1952; Vols. II and III, p 35; reprint of NBS Circular No. 467. (b) Pickerling, J.C.; Zilio, V. *Eur. Phys. J. D* **2001**, *13*, 181−185.

(40) Tjeng, L.; Vos, A.; Sawatzky, G. *Surf. Sci.* **1990**, *235*, 269−279.

(41) Marques, M. A. L.; Gross, E. K. U. *A Primer in Density Functional Theory*; Fiolhais, C., Nogueira, F., Marques, M. A. L., Eds.; Lecture Notes in Physics; Springer: Berlin, 2003; Vol. 620; pp 144−184.

(42) Pyykkö, P. *Chem. Rev.* **1988**, *88*, 563−594.

(43) Berglund, C. N.; Spicer, W. E. *Phys. Rev.* **1964**, *136*, A1044−A1064.

(44) Pampuch, C.; Rader, O.; Kachel, T.; Gudat, W.; Carbone, C.; Kläsges, R.; Bihlmayer, G.; Blügel, S.; Eberhardt, W. *Phys. Rev. Lett.* **2000**, *85*, 2561−2564.

(45) Matveev, A. V.; Neyman, K. M.; Yudanov, I. V.; Rösch, N. *Surf. Sci.* **1999**, *426*, 123−139.

(46) Albright, T. A.; Burdett, J. K.; Whangbo, M.-H. *Orbital Interactions in Chemistry*; Wiley: New York, 1985.

(47) Morse, M. D. *Chem. Rev.* **1986**, *86*, 1049−1109.

(48) Witko, M.; Beckmann, H. O. *Mol. Phys.* **1982**, *47*, 945−957.

(49) Das, K. K.; Balasubramanian, K. *J. Mol. Spectrosc.* **1990**, *140*, 280−294.

(50) Lochet, J. *J. Phys. B* **1978**, *11*, L55−L57.

(51) McCaffrey, J. G.; Bennett, R. R.; Morse, M. D.; Breckenridge, W. H. *J. Chem. Phys.* **1989**, *91*, 92−103.

(52) Page, R. H.; Gudeman, Ch. S. *J. Chem. Phys.* **1991**, *94*, 39−51.

(53) Ames, L. L.; Barrow, R. F. *Trans. Faraday Soc.* **1967**, *63*, 39−44.

(54) Simard, B.; Hackett, P. A. *J. Mol. Spectrosc.* **1990**, *142*, 310−318.

(55) Bonačić-Koutecký, V.; Pittner, J.; Boiron *J. Chem. Phys.* **1999**, *110*, 3876−3886.

(56) Beutel, V.; Krämer, H.-G.; Bhale, G. L.; Kuhn, M.; Weyers, K.; Demtröder, W. *J. Chem. Phys.* **1993**, *98*, 2699−2708.

(57) Wang, F.; Ziegler, T.; van Lenthe, E.; van Gisbergen, S.; van Baerends, E. *J. Chem. Phys.* **2005**, *122*, 204103, 1−13.